

Fracture parameters for sintered steels

YAN-BIN KE, BRIAN COTTERELL, YIU-WING MAI

Department of Mechanical Engineering, University of Sydney, Sydney, NSW 2006, Australia

Measurements of the plane strain fracture toughness K_{Ic} of sintered steels have frequently been invalid because the requirement that $P_{max}/P_Q < 1.1$ (where P_{max} = maximum load and P_Q = load used to calculate K_{Ic}) has not been met. We show that the reason for the criterion not being met is that sintered steels have a considerable crack growth resistance K_R . Values obtained in the past for K_{Ic} probably have been over-estimates of the initiation value of the crack growth resistance K_i and under-estimates of the maximum crack growth resistance K_{∞} . The important point is that the assessment of the toughness of sintered steels by a single parameter is not appropriate. Test methods to determine the crack growth resistance of sintered steels are discussed. Crack growth, which is difficult to detect by visual observation, can be determined by compliance techniques. Because of the porous nature of sintered steel, fatigue cracks are unnecessary at the tip of the notch and indeed are undesirable as they can easily cause errors in toughness measurements through inadvertent overloading. The thickness requirement for plane strain measurements can also be relaxed.

1. Introduction

Sintered iron and low-alloy steel components are primarily used because complex parts can be manufactured economically and accurately in large quantities. Typical uses of sintered iron and low-alloy steel are in automobiles, household machines and pumps. In these applications the mechanical properties of the material are important. However, the full potential of sintered metals has not been exploited for structural parts because less is known about their mechanical behaviour than the more usual wrought or cast metals.

Sintered metals have a porous structure with a typical porosity in the range of 5 to 20% so that the material has a density of 80 to 95% of that of the solid metal. Ultimate strengths similar to those of solid metals can be fairly easily achieved, but the ductility and toughness of sintered metals are limited. Fractures in sintered steel specimens with high porosity (> 20%) propagate with little plastic deformation through grain boundaries as evinced by the river patterns shown on the fracture surface [1]. The fracture surfaces of low-porosity specimens show transgranular fracture by microvoid coalescence. Cleavage fracture does occur in low-porosity specimens, but complete cleavage facets are almost absent. Since the yield strength of sintered metals is low when the porosity is high, the toughness of sintered steel increases with yield strength [2-5] in contrast to wrought steel where the toughness decreases with yield strength [6-8] as is illustrated in Fig. 1.

The toughness of sintered metals has been assessed either by an impact test [1] or by a plane strain fracture toughness test [2-5]. The results from impact tests cannot be used quantitatively in the design of sintered components, and the use of tests based on fracture mechanics is to be preferred. However, past workers

have found it difficult to perform valid plane strain fracture toughness tests according to the standard [9]. Undoubtedly the thickness requirement of the standard

$$B > 2.5 \left(\frac{K_{Ic}}{\sigma_y} \right)^2 \quad (1)$$

can be relaxed, because the constraint on plastic flow is determined by the pore geometry rather than the thickness of the specimen. More seriously, the requirement that the ratio of the maximum load P_m to the load P_Q used to calculate the plane strain fracture toughness K_{Ic} shall be less than 1.1, i.e.

$$P_m/P_Q < 1.1 \quad (2)$$

can rarely be met. In the standard plane strain fracture toughness test this requirement makes sure that the non-linearity in the force-displacement diagram is due to crack growth rather than plastic flow or to a considerable increase in crack growth resistance with crack extension. Linear elastic fracture mechanics can apply if the ratio P_m/P_Q exceeds 1.1 because of crack growth resistance rather than plastic flow, but it is not then appropriate to characterize the toughness of the material by the initiation plane strain fracture toughness. For such materials it is necessary to determine the crack growth resistance curve in order to predict accurately their mechanical behaviour.

It had been observed that in a tension test on an unnotched sintered iron specimen (porosity \approx 18%) that cracks are initiated at stresses less than the nominal yield strength [10]. As the stress increases these cracks grow stably, and more and more cracks are initiated until just before fracture there are a multitude of cracks present. Such behaviour could not occur unless there was a significant increase in resistance to cracking with crack growth. Similar evidence

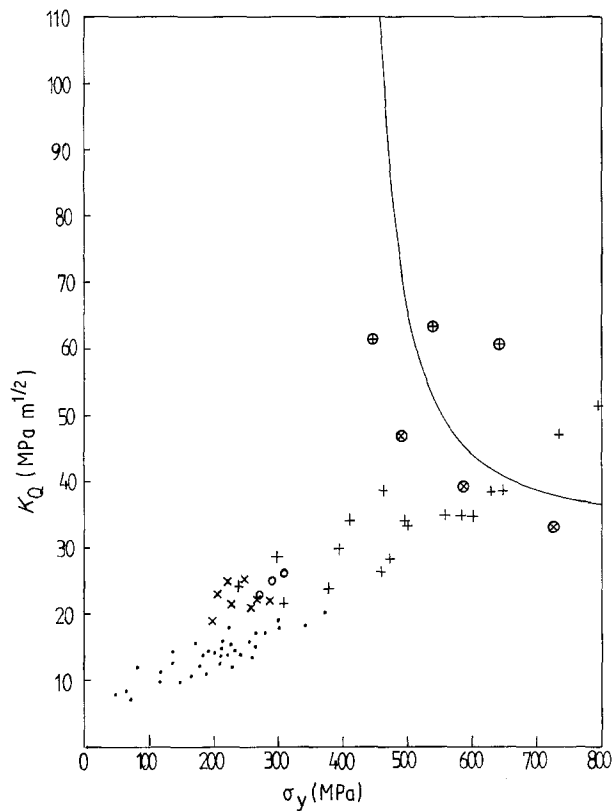


Figure 1 Published values of fracture toughness as a function of yield strength for sintered and wrought steels. Sintered steels: (●) [2], (×) [3], (+) [4], (○) [5]; wrought steel: (—) [6], (⊕) [7].

of the existence of a crack growth resistance curve was obtained [11] in tests on the Williams split nut sintered from a Höganäs phosphorus-containing steel powder PNC45. In this test small cracks were observed at the root of the threads at a stress of about 650 MPa (based on the effective area of the bolt) which was far below the failure stress of about 950 MPa.

The crack growth resistance curve for a sintered steel is shown schematically in Fig. 2. The resistance to crack propagation rises from an initiation crack growth resistance K_i to a plateau value K_∞ provided the specimen is large enough. For smaller specimens, the crack growth resistance curves for materials other than sintered steels are in general dependent on size and geometry and may not even reach a flat plateau [12, 13]. The crack growth resistance curve concept was first applied to a high-strength aluminium alloy sheet where the increase in resistance was primarily due to a transition from plane strain to plane stress and the development of shear lips [14]. However, the resistance to crack growth can increase even when there is no transition and the fracture surface remains transverse and flat as it does in sintered metals [15].

This paper gives the preliminary results of an investigation into the crack growth resistance curve for a sintered steel and the appropriate methods for its measurement.

2. Measurement of the crack growth resistance curve for a sintered steel

The ASTM has issued a standard that gives the method of determination of crack growth resistance curves for metallic materials [16] which we have basically followed. Because dies existed for disc-shaped speci-

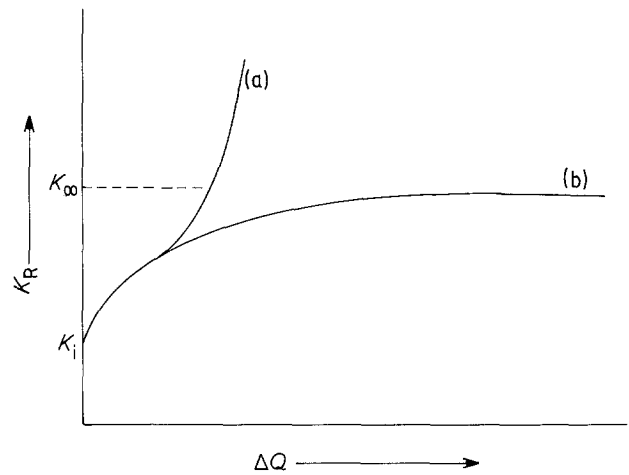


Figure 2 Schematic crack growth resistance curves: (a) small notch bend specimen, (b) large specimen.

mens we have chosen the standard disc-shaped compact tension specimens, DC(T), for our tests [9]. The general dimensions of the DC(T) specimen are shown in Fig. 3.

In these preliminary tests we have tried to measure the crack growth resistance in as standard a way as possible. The crack growth resistance curve standard [16] does not have a thickness requirement because it is designed for determining the crack growth resistance of thin, high-strength metals where the increase in crack growth resistance is due to a plane strain-plane stress transition. However, because the increase in crack growth resistance in sintered steel is not the result of such a transition, we desired to obtain a reference resistance curve that is essentially independent of geometry and size effects and is therefore a material property. Although for wrought or cast metallic materials the thickness requirement given by Equation 1 would need to be satisfied, we believe in common with many investigators [3, 5] that this requirement can be relaxed for sintered steels because the constraint on plastic flow is governed by the shape of the necks between the sintered particles rather than the thickness of the specimen. However, to obtain a reference crack growth resistance curve that is independent of geometry it is important that the plastic zone size is small compared with the dimensions of the specimen. The requirement of the plane strain fracture toughness test ensures that the crack and remaining ligament lengths are about fifty times the radius of the plastic zone r_p . With sintered steel the plane stress relationship for the radius of the plastic zone [17],

$$r_p = \frac{1}{2\pi} \left(\frac{K}{\sigma_y} \right)^2 = 0.159 \left(\frac{K}{\sigma_y} \right)^2 \quad (3)$$

is more appropriate than the plane strain relationship because the flow stress determined from a simple tension test is the flow stress that applies at the tip of a crack. Hence, the crack length (a) and the ligament length ($W - a$) should preferably both satisfy the inequalities

$$a, (W - a) > 50r_p \quad (4)$$

However, we shall see that in practice it is difficult to

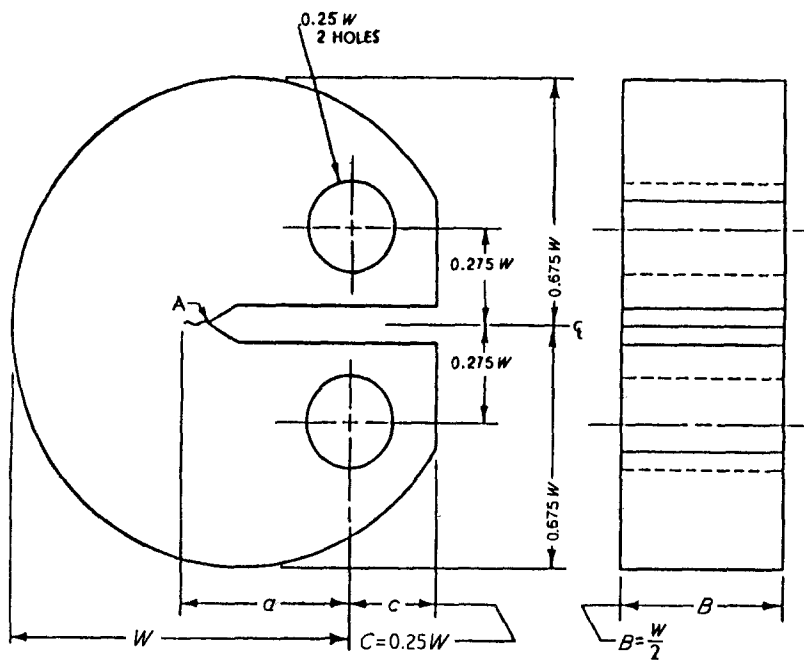


Figure 3 General dimensions of the disc-shaped compact tension specimen DC(T). A is the machine notch tip.

satisfy the above inequality. The size requirement of the crack growth resistance standard [16] is less restrictive than Equation 4 and only requires that

$$a, (W - a) > \frac{4}{\pi} \left(\frac{K_{\infty}}{\sigma_y} \right)^2 \quad (5)$$

With high-strength wrought or cast metallic materials it is necessary to have a very sharp crack tip or the indicated value of K_R will be larger than the true values. It has been argued by Fleck and Smith [5] that crack initiation is determined by the radius of curvature of the necks between sintered particles and therefore sharp fatigue cracks are unnecessary. This argument is supported by the experiments of Barnby *et al.* [2] who showed that no difference could be detected between the fracture toughness measured using fatigue cracks and machined notches with a root radius of 0.1mm. Fatigue cracks are difficult to grow at the low stress intensity ranges required by the standards [2] and greatly increase the cost of the specimens; it is desirable to use machined notches if these give valid results. Hence we believe that the maximum permissible machined root radius should be determined.

It is difficult to detect crack growth on the surface of a sintered steel specimen and we believe that the compliance method of measuring crack growth as outlined in the standard [16] is to be preferred. In this method the compliance of the specimen is measured by partially unloading the specimen after every crack growth increment (Fig. 4). The compliances given by Newman [18] for the DC(T) specimen can then be used to measure the crack growth. In addition the effective crack length, that is the physical crack length plus the radius of the plastic zone, is obtained from the total compliance of the specimen V/P where V is the total crack mouth opening and P the load.

The value of K_R is calculated from the applied load and the effective crack length obtained from the compliance measurements from the expression for the stress intensity factor given by Newman [18].

3. Experimental results

3.1. The material

The composition of the sintered steel used in these tests is 0.82% carbon and 1.9% copper and is typical of composition of sintered steel used for automobile parts. The iron powder used was Mannesmann Demag (Sweden) WPL200. Discs 114.5 mm in diameter and approximately 22 mm thick were compacted with a pressure of 415 MPa. The specimens were sintered in an endothermic gas with a dewpoint of 0°C for 40 min in the temperature range 1079 to 1123°C. After sintering the average density of the specimens was 6700 kg m⁻³.

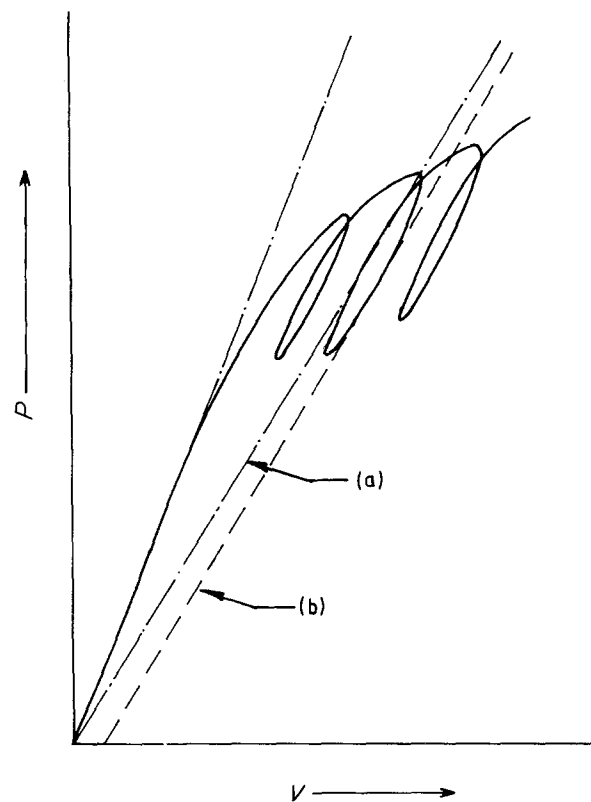


Figure 4 Schematic load-displacement curve for DC(T) specimen: (a) total compliance, effective crack length; (b) unloading compliance, physical crack length.

TABLE I Mechanical properties of sintered steel

Density (kg m^{-3})	Porosity (%)	E (GPa)	0.2% proof stress (MPa)	Ultimate strength (MPa)	Elongation (%)
6700	15.2	55.8	300	371	1.17

Tensile specimens were machined from the broken halves of the DC(T) specimens and the average results of the tension tests are given in Table I. The stress-strain curves were not linear in the elastic range and it was difficult to estimate Young's modulus. Consequently Young's modulus was inferred from the compliance measurements of the DC(T) specimens, and these inferred values are included in Table I.

3.2. Compliance measurements

The compliance of a DC(T) specimen of diameter 114.5 mm was compared with the theoretical values given by Newman [18] for a range of notch lengths ($a/W = 0.2$ to 0.8) machined with a 0.15 mm blade. Absolute comparison of the compliances was impossible because the Young's modulus of the sintered steel could not be measured accurately from the tension tests. Therefore the procedure adopted was to determine the effective Young's modulus by assuming that the compliance was accurately predicted by the theoretical solution for the shortest notch ($a/W = 0.2$) and then using this value to calculate the parameter EBV/P for the other notch lengths. The results of this comparison are shown in Fig. 5.

Further confirmation of the accuracy of the compliance method was obtained from measurement of the compliance of the crack growth resistance curve specimens after fatigue cracks had been intro-

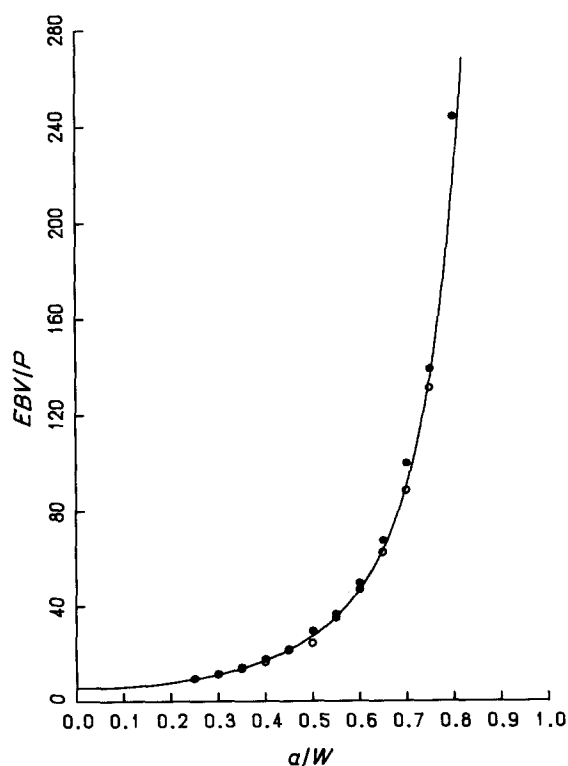


Figure 5 Theoretical and (○, ●) experimental compliance curves for DC(T) specimen.

duced. The extent of the fatigue crack growth could be measured directly after the specimens were fractured. The discrepancy between the estimates of fatigue crack growth from compliance measurements and physical measurement was not more than 0.05 mm.

3.3. Crack growth resistance curves

So far only one size of DC(T) specimen (114.5 mm in diameter) and approximately 22 mm thick has been tested. The starting notch was of three types; (a) a machined notch of 60° included angle cut with a milling cutter, producing a tip radius of approximately 0.2 mm; (b) a 0.3 mm wide slot cut by electric discharge machining; and (c) a machined notch with a fatigue crack extension. To promote early fatigue crack initiation the specimens were preloaded in compression to the maximum stress intensity factor K_{fmax} used to produce the fatigue crack. The stress intensity factor range ΔK_f was set at 90% of K_{fmax} . The specimens were fatigued in an electromagnetic resonance machine where the mean stress was applied mechanically through a screw. Since this screw was not adjusted during fatigue, the mean load decreased as the fatigue crack grew and the specimen became more compliant. This drop in mean load was used to determine the number of cycles for crack initiation. The maximum stress intensity factors at the beginning and end of the fatigue cycling are given in Table II. The first fatigue crack was formed with a maximum fatigue stress intensity factor of $14.4 \text{ MPa m}^{1/2}$, which is less than 60% of K_Q . However, subsequently we discovered that the actual value of the fracture initiation toughness K_i was actually less than $14.4 \text{ MPa m}^{1/2}$ and that the crack growth resistance curve from this specimen was significantly higher than that obtained for the other two specimens with notches sharpened by fatigue at a K_{fmax} of $6.1 \text{ MPa m}^{1/2}$ or less.

The crack growth resistance curves for the three notch types shown in Fig. 6 were calculated from the load-displacement curves by using the total compliance to calculate the effective crack length and the compliance on unloading to calculate the physical crack growth. Table II lists the crack growth resistance K_i at initiation obtained by extrapolation to zero crack extension, the plateau value of the crack growth resistance K_∞ , and also K_Q obtained for a 5% secant line as described in the plane strain fracture toughness standard [16].

4. Discussion of results

It is seen from Fig. 5 that the physical crack growth can be accurately predicted from compliance measurements if an effective elastic modulus is used. The correction to the physical crack size to account for plastic deformation r_p obtained from compliance measurements is plotted against $(K_R/\sigma_y)^2$ in Fig. 7. As expected the relationship is approximately linear (the

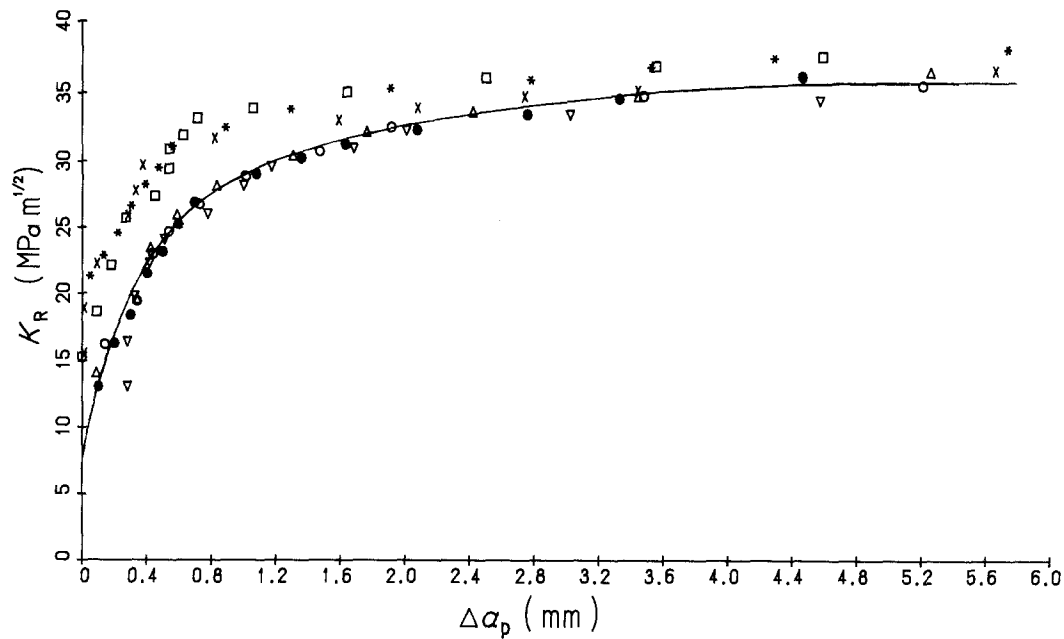


Figure 6 Crack growth resistance curve for sintered steel. (O, ●) Wire-cutting specimens, $r = 0.15$ mm; (Δ , ∇) fatigue precracking specimens, (*) overloaded; (\times , \square) machine-notched specimens, $r = 0.2$ mm.

correlation coefficient is 0.92) with a slope of 0.086. This value is nearly half (0.54) that predicted by Equation 3 on the assumption that the plastic flow constraint in the DC(T) specimen is the same in a plain tension test, but it is more than one and a half times the size of the plane strain correction factor

$$r_p = \frac{1}{6\pi} \left(\frac{K_R}{\sigma_y} \right)^2$$

Hence the notch in a DC(T) specimen does provide some constraint against plastic flow.

The crack growth resistance curves for the two fatigue crack sharpened notches that used the lower K_{fmax} (Specimens 12 and 19) and the electric discharge machined notches of radius 0.15 mm (Specimens 9 and 10) are essentially the same. However, the crack growth resistance curves for the higher fatigue load (Specimen 3) and those specimens with conventionally machined notches of radius 0.2 mm (Specimens 14 and 30) are significantly higher. The value of K_Q obtained by the method outlined in the plane strain fracture toughness standard [16] is significantly higher than K_I obtained by extrapolating from the crack growth resistance curves. The values of K_Q would not be valid K_{Ic} values according to the standard because the inequality $P_m/P_Q < 1.1$ is not satisfied. However, P_m/P_Q is in the same range as observed in toughness tests by other workers [2-5] so one must assume that the initial

value K_I is lower and the plateau value K_{∞} of the crack growth resistance curve is higher than the values of the plane strain fracture toughness quoted by these workers.

If we use the experimentally determined relationship for r_p then the minimum crack (a) and ligament (W/a) lengths according to Equation 4 are about 58 mm, so that the specimen size is marginally too small to satisfy this inequality. However, the minimum crack (a) and ligament lengths ($W - a$) according to Equation 5 are only 17.3 mm. Hence it is likely that the reference crack growth resistance curve is reasonably accurate. The effect of varying the specimen size will be determined in future work.

5. Conclusions

Because sintered metals show a significant increase in toughness with crack extension it is inappropriate to attempt to characterize the fracture behaviour with a single parameter. If K_Q is measured by the plane strain fracture toughness method, it is larger than K_I and less than K_{∞} . Only a full crack growth resistance curve will enable the full fracture behaviour of a sintered component to be predicted.

Sharp machined notches can be used instead of fatigue cracks. Indeed, from the present tests they are to be preferred because of the danger of artificially increasing K_R if the fatigue load is too large. The

TABLE II Crack growth resistance data

Specimen No.	Notch radius (mm)	K_{fmax} (MPa m ^{1/2})		P_m/P_Q	K_Q (MPa m ^{1/2})	K_I (MPa m ^{1/2})	K_{∞} (MPa m ^{1/2})
		Initial	Final				
3	-	14.2	14.4	1.12	27.9	19.0	39.0
9	0.15	-	-	1.26	23.5	11.5	35.6
10	0.15	-	-	1.27	22.8	8.8	36.3
12	-	5.9	6.1	1.32	21.9	10.3	37.6
14	0.21	-	-	1.13	26.5	15.2	37.3
19	-	5.2	5.3	1.23	23.3	10.3	34.7
30	0.20	-	-	1.12	28.1	15.2	39.3

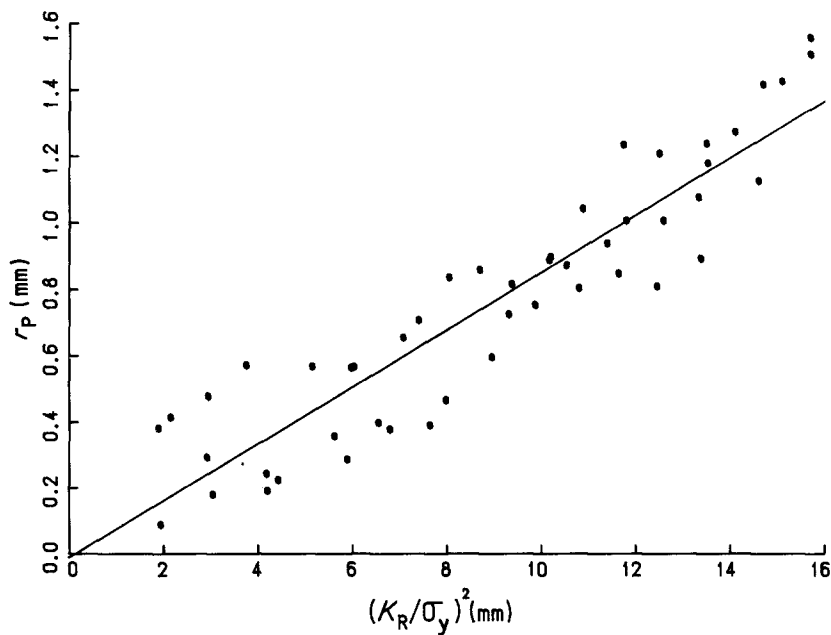


Figure 7 Plasticity correction-factor r_p as a function of $(K_R/\sigma_y)^2$: (●) experimental, (—) $r_p = 0.086 (K_R/\sigma_y)^2 - 0.01$ (correlation coefficient 0.92).

maximum notch root radius that will give a valid K_R curve has not yet been determined, but the value of 0.1 mm already quoted by Barnby *et al.* [2] does not seem unconservative from the present tests. More attention will be paid to this important topic in future work.

Acknowledgements

We thank Astra Engineering and especially Mr Malcom Evans and Mr Bill Hughes for the loan of the compaction die, supplying the metal powders and performing the sintering operation. Y.-B Ke also wishes to thank the University of Sydney for the award of a Post-graduate Research Scholarship when this work was done.

References

1. P. RAY and G. S. TENDOLKAR, *Planseeber. Pulvermetall.* **24** (1976) 198.
2. J. T. BARNBY, D. C. GHOSH and K. DINSDALE, *Powder Metall.* **16** (1973) 55.
3. A. De IORIO, in "Modern Developments in Powder Metallurgy", Vol. 13 (Metal Powder Industries Federation, Princeton, 1981) pp. 229-246.
4. N. INGELSTRÖM and V. USTIMENKO, *Powder Metall.* **18** (1975) 303.
5. N. A. FLECK and R. S. SMITH, *ibid.* **24** (1981) 121.
6. D. J. SEMAN, G. P. KALLENBERG and R. J. TOWNER, Report WAPD-TM-895 (Bettis Atomic Powder Lab,

- Pittsburgh, Pennsylvania, 1971).
7. W. G. CLARK and E. T. WESSEL, ASTM STP 463 (American Society for Testing and Materials, Philadelphia, 1970) p. 160.
8. J. MALKIN and A. S. TETELMAN, *Engng Fract. Mech.* **3** (1971) 151.
9. ASTM Standard E399-1981, "Standard Test Method for Plane Strain Fracture Toughness of Metallic Materials" (American Society for Testing and Materials, Philadelphia, 1981).
10. H. E. EXNER and D. POHL, *Powder. Metall. Internat.* **10** (1978) 1194.
11. B. COTTERELL, *Engng. Designer* (1988) in press.
12. Y.-W. MAI, *Mater. Forum.* (1988) in press.
13. B. COTTERELL and Y.-W. MAI, *ibid.* (1988) in press.
14. J. M. KRAFFT, A. M. SULLIVAN and R. W. BOYLE, in Proceedings of Crack Propagation Symposium, College of Aeronautics, Cranfield, 1961, Vol. 1, p. 8.
15. J. R. RICE, in "Proceedings of Conference on Mechanics and Mechanisms of Crack Growth, 1975, edited by M. J. May, British Steel Corp., Physical Metallurgy Centre Report, p. 14.
16. ASTM Standard E561-81, "Standard Practice for R-Curve Determination" (American Society for Testing and Materials, Philadelphia, 1981).
17. G. R. IRWIN and J. E. SRAWLEY, *Mater. Prüfung* **4** (1962) 1.
18. J. C. NEWMAN, "Stress-intensity factors and crack-opening displacements for round compact specimens", NASA Technical Memorandum 80174 (1979).

Received 9 September
and accepted 10 December 1987